Surface exposure dating and geophysical prospecting of the Holocene Lauvitel rock slide (French Alps)

Romain Delunel, Didier Hantz, Regis Braucher, D.L. Bourles, Philippe Schoeneich, Jacques Deparis

Landslides (2010) 7:393–400
DOI 10.1007/s10346-010-0221-0
Received: 28 October 2009
Accepted: 11 May 2010
Published online: 28 May 2010

Romain Delunel · Didier Hantz · Régis Braucher · Didier L. Bourlès · Philippe Schoeneich · Jacques Deparis

Surface exposure dating and geophysical prospecting of the Holocene Lauvitel rock slide (French Alps)

Abstract Large rock falls and rockslides represent a risk for human communities in mountainous areas as they can cause fatalities and destruction of settlements and infrastructures. Assessing the associated hazard requires constraining the time frequency of such events. Since large rockslides are not common, estimating their frequency requires recording them over a long period of time. The Holocene period then appears as pertinent, which implies that rockslide features have to be dated with absolute chronology methods. This paper presents a characterisation and dating of the Lauvitel rockslide, one of the largest Holocene rockslides in the French Alps. Combining field observation with electrical tomography profiles performed on the rockslide deposit that constitutes the Lauvitel Lake dam allows estimating its volume at a minimum of 12×10^6 m^3. In addition, cosmic ray exposure dating using in situ-produced ^{10}Be concentration measurements has been applied to date seven samples collected both on the main sliding surface and on blocks lying on the dam and further downstream. Ages obtained are consistent with a single large rockslide event, which occurred at 4.7 ± 0.4 ^{10}Be-ka and formed two distinct deposits. However, from a mechanical point of view, these clearly separated deposits could hardly result from a single movement. A comparison of their reach angles with those reviewed in the literature highlights that the lower deposit must result from rock avalanches larger than 10^7 m^3, while the upper one (the Lauvitel dam) must result from several events smaller than 10^6 m^3. In the context of hazard assessment for land use planning, these events can, however, be considered as a unique event.

Keywords Cosmic ray exposure dating · Electrical tomography · Lauvitel dam · Ecrins-Pelvoux massif

Introduction

Rock falls and most rockslides are extremely rapid mass movements representing a risk for human communities in mountainous areas: Rock falls smaller than 1 m^3 may cause fatalities while larger ones may destroy human settlements. In order to assess the hazard associated with such events in land use planning, potential rock falls have to be identified and characterised, and their probability of occurrence has to be evaluated on a given period of time (Fell et al. 2005; Picarelli et al. 2005). For land use planning purposes, the period of time to be considered is on the order of ~100 years. In the current state of knowledge, there is no reliable mechanical method that is able to predict the future behaviour of a stable rock slope, even in a probabilistic way (Hantz and Frayssines 2007). Therefore, rock fall/slide hazard assessment is usually limited to qualitative approaches. Recently, some authors have proposed to use historical inventories in order to assess rock fall/slide hazards in a quantitative way (Dussauge-Peisser et al. 2002; Hantz et al. 2003; Moon et al. 2005). This quantitative approach is based on the knowledge of the rock fall/slide frequency within a particular area. The time period considered for such inventories must, however, be long enough to provide a significant estimate of the mean frequency. Two types of inventory can be distinguished. The first is based on historical records, which usually cover 10^1 to 10^2 years and is appropriate for volumes ranging from ~10^0 to 10^5 m^3 (e.g. Dussauge-Peisser et al. 2002). The second is based on the recognition of large Holocene events representative of larger volumes: Hungr and Evans (2004) presented time frequency of rock falls larger than 20×10^6 m^3. More detailed field investigations are necessary to achieve such inventories for smaller volumes, distinguishing homogeneous areas according to their geomorphic settings. Using such a resulting frequency in hazard assessment supposes that rock fall frequency remains constant during the Holocene. Data from a new Alpine rock fall inventory support this view (Schoeneich et al. 2008). However, some authors suggest that rock avalanche frequency may have been higher during the early Holocene due to different climatic forcing (Cruden 1995; Ballantyne 2002; Ivy-Ochs et al. 2009). Ongoing climate change may thus influence rockslide frequency (Climchalp 2008a, b). Therefore, it appears essential to date Holocene rockslides to assess the potential relation between climate and geological setting on rock fall occurrence rate. Finally, in order to construct magnitude–frequency relationships, the frequency has to be determined for different slide magnitudes; it is also important to determine the volume of each event.

This paper focuses on the Lauvitel rockslide where geophysical prospecting and cosmic ray exposure (CRE) dating were performed in order to constrain both its volume and age. The volume was determined by estimating deposit thickness and aerial surface through geophysical and geomorphological surveys. The age of the event was determined through CRE dating using in situ-produced ^{10}Be concentration measurements of samples collected on features associated with the rockslide. Rock avalanches have generally been dated with the radiocarbon method (cf. Schoeneich et al. 2008 for a review), but this method requires organic matter (i.e. wood or charcoal) to be found within the deposit. Such an important constraint is not required when using CRE dating. Recently, several rock slides have been dated with this method, using ^{36}Cl for limestone (Soldati et al. 2004; Van Husen et al. 2007; Ivy-Ochs et al. 2009; Prager et al. 2009) and ^{10}Be for quartz-bearing rocks (Cossart et al. 2008; Hormes et al. 2008; Le Roux et al. 2009).

The Lauvitel rockslide

The Lauvitel valley is a 7-km-long tributary of the Vénéon River, one of the main rivers draining the Ecrins–Pelvoux massif. This massif belongs to the External Crystalline Massifs of the Western Alps and is located about 50 km southeast of Grenoble (Fig. 1). The 68-m-deep Lauvitel Lake lies upstream of a natural dam at an elevation of 1,500 m (Fig. 2). The origin of this lake has been

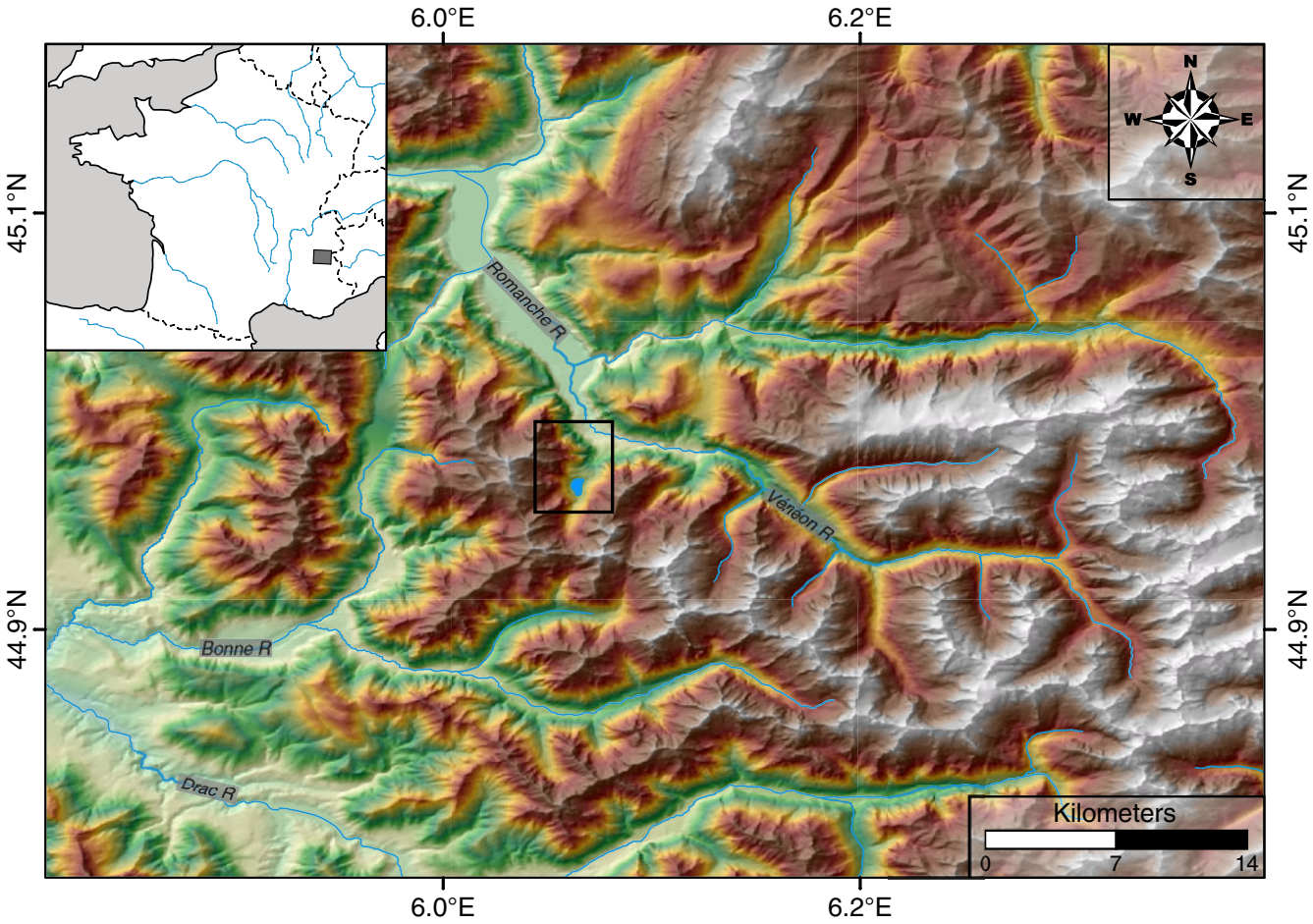

Fig. 1 Digital Elevation Model (©Institut Géographique National, 50-m resolution) of the western part of the Ecrins–Pelvoux massif. *Black box* indicates location of Fig. 2. *Inset* shows location within France

diversely interpreted within the literature. Kilian (1922) and Monjuvent (1978) interpreted the dam as a frontal moraine of the Lauvitel glacier, and they also described lateral moraines downstream of the dam. Moreover, Kilian (1922) described an earlier moraine at the bottom of the Vénéon valley, which is interpreted by Monjuvent as a frontal moraine of the Vénéon glacier. These moraines should have been deposited during the Late glacial stage (~15–12 ka B.P.). For Delebecque (1898) and Abele (1974), the dam is the deposit of a large rock slide, the scar of which is clearly visible on the left side wall of the Lauvitel valley (Fig. 3). Many arguments support the rockslide hypothesis rather than a glacial origin: first, the prominent scar dominating the dam to the west; second, the gentle but obvious slope of the deposit from the west wall towards the opposite valley side; third, the coarse blocky shape of the deposit and its homogeneous petrography, which is the same granite as the scar, whereas this lithology is nearly absent in the upper catchment; and finally the large lake-level fluctuations. The lake's level varies seasonally by ca. 25 m due to the porosity of the dam. Apart from the lithology, the morphological setting and hydrological properties largely resemble the Oeschinensee dam (Swiss Alps), which is a rock avalanche dam (Niklaus 1967). Abele (1974) suggested that the sliding mass split up in two parts, the upper one forming the dam and the lower one propagating down to the Vénéon, where Kilian (1922) described a moraine. According to this hypothesis, Abele (1974) estimated a total rockslide volume of 75×10^6 m^3. Considering this volume, the Lauvitel rockslide/avalanche could be the largest rockslide known in the Ecrins–Pelvoux massif and belong to the largest rockslides or rock avalanches identified within the crystalline massifs of the European Alps (Schoeneich et al. 2008).

From a geotechnical point of view, the west wall of the Lauvitel valley consists of granite and comprises three joint sets with the following mean dip direction/dip and spacing: J1 (90/58, 1 m); J2 (190/80, 1 m); and J3 (270/60, 100 m). The joint set J1 is roughly parallel to the initial valley wall. The sliding surface (Figs. 2 and 3) occurs from 2,400 m to 1,700 m and is mainly defined by J1 joints. It dips 57° in its upper part (2,387 m to 1,907 m), 45° in its medium part (1,907 m to 1,840 m) and 50° in its lower part (1,840 m to 1,709 m). At first sight, the slide could be classified as a translational one, but the variations in inclination of the sliding surface lead to its classification as a compound slide. The reach angles (Heim 1932) corresponding to the upper and lower deposits are 33° and 19°, respectively.

Geophysical survey of the dam

Two electrical tomographic profiles were collected: (1) profile 1 (A–B; Figs. 2 and 4) runs along the crest of the dam for ~700 m across the valley and (2) profile 2 (C–D; Figs. 2 and 4) runs

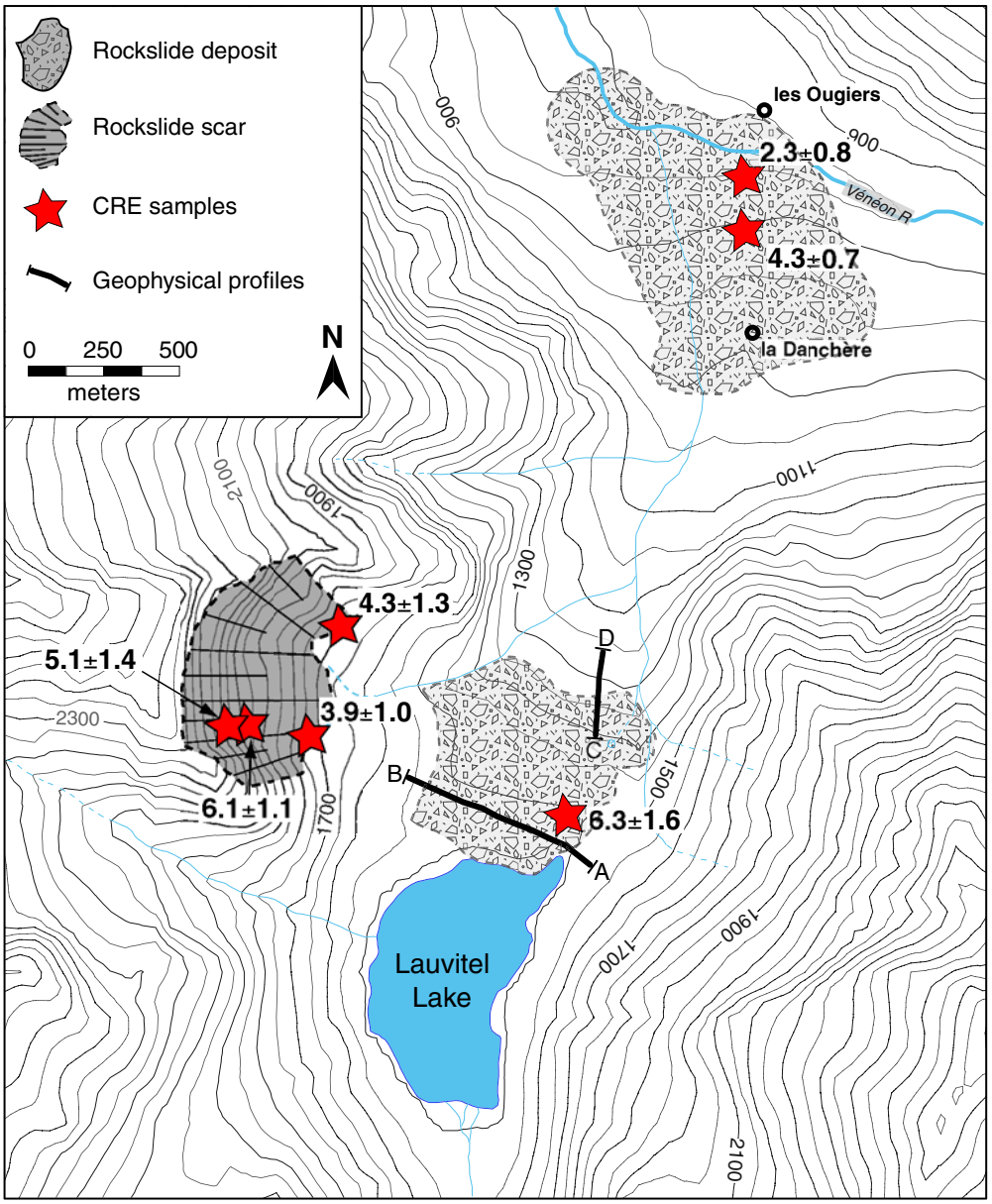

Fig. 2 Location of the Lauvitel rockslide features, samples location, ^{10}Be exposure ages (ka) and geophysical profiles

parallel to the valley axis along ~300 m. Profile 2 crosses the supposed lower limit of the dam, characterised by a sudden change in slope inclination where many springs are located. Both profiles were acquired using a Wenner configuration and 64 electrodes spaced every 5 m. Data of profile 1 were gathered, as they were recorded using a roll-along technique every 16 electrodes. The inversed profiles are shown in Fig. 4 after suppressing aberrant resistivity values obtained due to bad coupling between electrodes and the sometimes rocky material. They were derived using the RES2DINV software with a L1 regularisation norm and are presented after three iterations, satisfying root mean square error values.

On top of profile 1 (Figs. 2 and 4), the three different formations visible on the surface are characterised by different resistivities. On the northwestern side, the scree corresponds to values ranging between 3,500 and 5,000 Ω m. On the southeastern side, an alluvial fan is characterised by resistivities between 2,500 and 4,000 Ω m. In the central part of the profile, the rockslide deposit has a resistivity higher than 5,000 Ω m. This can be explained by its high porosity, which is implied by the accumulation of large blocks (typical size of a few cubic-metres scale).

The thickness of this latter formation is about 10 m below the eastern part of the dam and reaches up to 50 m below its western part, with a resistivity much higher than 5,000 Ω m. Below this surficial layer, resistivity decreases with depth, indicating finer and wetter material that could be morainic. In the eastern part of the profile, the lower resistivity (1,000 Ω m) observed at the elevation of about 1,500 m, which roughly corresponds to the lake level at the time of geophysical survey (1,490 m, 31 August 2005; D. Dumas personal communication), can be explained by the water-table position. The deeper occurrence of the water saturation signal in the northwestern part could be due to the longer distance

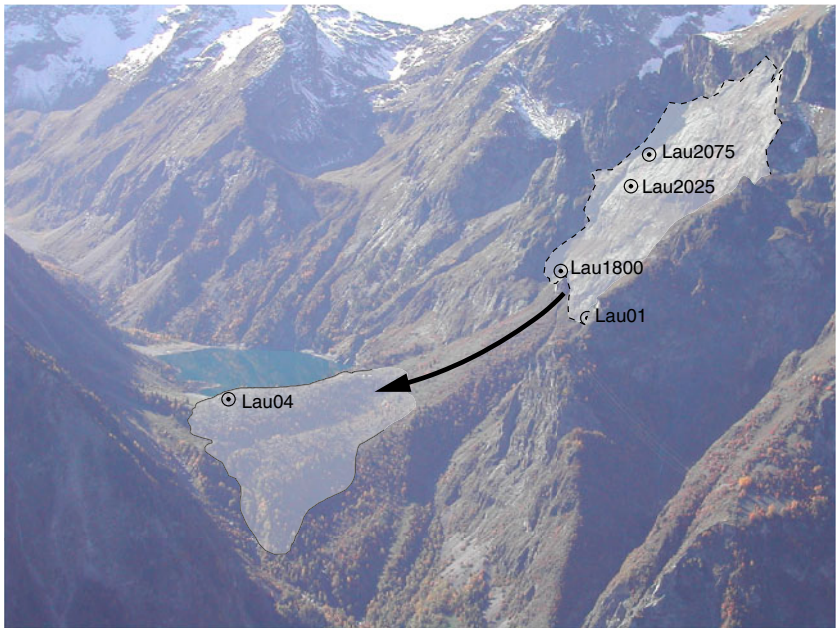

Fig. 3 General southward view of the Lauvitel valley. *Light shaded areas* correspond to (**a**) primary rock slide plane (*up*) and (**b**) upstream rock avalanche deposit (*down*). The Lauvitel lake is clearly visible upstream of the dam. The five highest sample locations are also represented

from the lake. The high resistivity zone (7,500–10,000 Ω m) on the eastern lower part of the profile (Fig. 4) is interpreted as an edge artefact of the inversion due to fewer data underneath.

Contrarily to profile 1, the nature of the ground surface was less visible on profile 2 due to vegetation cover. However, the resistivity values clearly show two different types of material below the surface. The upper and steeper part (i.e. the northern part; Figs. 2 and 4), which has an approximate thickness of 40–50 m, corresponds to a similar resistivity range as the surficial layer in profile 1 (i.e. higher than 5,000 Ω m). The lower part shows mostly low resistivity values (i.e. <1,000 Ω m, Fig. 4) as for the saturated materials previously described. These two forma-

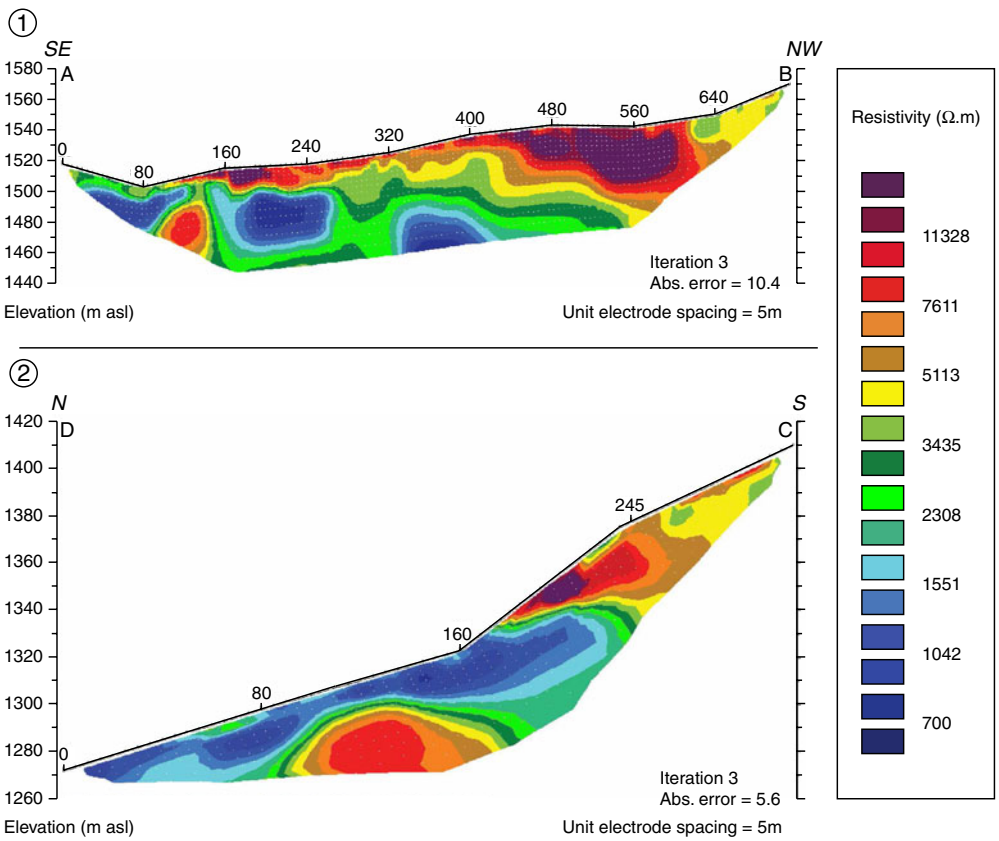

Fig. 4 Resistivity cross-sections obtained from electrical tomography profiles located in Fig. 2. Tomography profiles were performed using Syscal R1 PLUS resistivity meter (Iris Instrument©) with a Wenner electrode array configuration. Data inversions were performed through RES2DINV software according to a robust inversion method (Claerbout and Muir 1973). Values represented along profile surfaces correspond to distance in metres

tions are interpreted as the rockslide deposit and the moraine identified in profile 1, respectively. A relatively high resistivity zone (7,500–10,000 Ω m) appears under the saturated moraine at a depth of 10–20 m, which can be interpreted as bedrock. Considering these two electrical tomography profiles, the base of the deposit would fall from an elevation of 1,500 m in the southeastern part of profile 1 to ~1,330 m in the centre of profile 2 where it crosses the surface (Fig. 4). However, the area that connects these two locations cannot be directly inferred from our electrical tomography profiles.

Geophysical prospecting has been used to confirm the supposed lower limit of the upper deposit, which was previously determined through geomorphological evidence. The projected surface of the upper deposit (Fig. 2) is estimated to be $40\times10^4 m^2$. Along the geophysical profiles, its mean thickness varies between 10 and 50 m. From the examination of the profiles and the geomorphological map, the mean thickness can reasonably be estimated at 30±10 m, leading to an approximated volume of $12 \pm 4 \times 10^6 m^3$. This has to be considered as a minimal value, as the low resistivity values due to the supposed water table can lead to an underestimation of the real thickness of the deposit.

Cosmic ray exposure dating

Sampling locations

Seven samples were collected during summer 2005 (Figs. 2 and 3). Samples Lau2075, Lau2025 and Lau1800, whose index refers to the sampling elevation, were collected on the clearest main sliding planes (Fig. 3) where the dip is about 60°. Considering the topography of the scar (Figs. 2 and 3), these samples were probably shielded by several tens of metres of rock before the slide occurred. Lau01 was taken in the scar near its assumed northern limit, on a 70° dipping plane. Lau04 was sampled on the top of a block located on the middle of the dam surface, downstream from the main scar but sufficiently far from it to reject the hypothesis of a single block fallen later than the main event. Lau10 and Lau11 (Fig. 2) were collected on separate blocks located on the lower deposit described by Abele (1974). All samples are granite and were collected with hammer and chisel from the uppermost 5 cm of the rock surface.

Sample preparation, analysis and cosmic ray exposure age calculation

Samples were prepared for accelerator mass spectrometry (AMS) ^{10}Be measurements following chemical procedures adapted from Brown et al. (1991) and Merchel and Herpers (1999). Samples were crushed and sieved; 250–1,000 m fractions were conserved for chemical procedures. Pure quartz grains were obtained by repeated H_2SiF_6–HCl etching and atmospheric ^{10}Be content eliminated by successive HF sequential dissolutions. Prior to the complete HF digestion of quartz grains, addition of a weighted 300 µl of 10^{-3}g g^{-1} Be carrier solution allowed to fix the ^{10}Be/^{9}Be ratio of samples. Remaining solutions were dried, diluted in HCl and purified on anion and cation exchange columns, and Be was extracted by alkaline precipitations. BeO targets were finally prepared for AMS ^{10}Be measurements performed with the 3 MV Tandétron facility at Gif-sur-Yvette, France (Raisbeck et al. 1987, 1994). The presented data were calibrated against 07KNSTD using a ^{10}Be half-life of $(1.36 \pm 0.07) \times 10^6$ years (Nishiizumi et al. 2007).

In order to determine CRE ages from the ^{10}Be concentrations measured in the quartz fractions, the following equation was used:

$$C_{(x,\varepsilon,t)} = C_0 \cdot e^{-\lambda t} + \frac{P_{spal}}{\frac{\varepsilon}{\Lambda_n}+\lambda} \cdot e^{-\frac{x}{\Lambda_n}}\left[1 - e^{-t\left(\frac{\varepsilon}{\Lambda_n}+\lambda\right)}\right] + \frac{P_{\mu s}}{\frac{\varepsilon}{\Lambda_{\mu s}}+\lambda} \cdot e^{-\frac{x}{\Lambda_{\mu s}}}\left[1 - e^{-t\left(\frac{\varepsilon}{\Lambda_{\mu s}}+\lambda\right)}\right] + \frac{P_{\mu f}}{\frac{\varepsilon}{\Lambda_{\mu f}}+\lambda} \cdot e^{-\frac{x}{\Lambda_{\mu f}}}\left[1 - e^{-t\left(\frac{\varepsilon}{\Lambda_{\mu f}}+\lambda\right)}\right]$$

where $C_{(x,\ \varepsilon,\ t)}$ is the ^{10}Be concentration as a function of depth x (g cm^{-2}), ε is the erosion rate and t the exposure time (years); C_0 is the potential ^{10}Be inherited concentration prior to exposition at the surface; Λ_n, $\Lambda_{\mu s}$ and $\Lambda_{\mu f}$ are the effective apparent attenuation lengths (g cm^{-2}) for neutrons, slow muons and fast muons, respectively. P_{spal}, $P_{\mu s}$ and $P_{\mu f}$ are the spallogenic, slow and fast muon production rates, respectively, that contribute to the total ^{10}Be production. All calculations were performed using attenuation lengths of 150, 1,500 and 5,300 g cm^{-2} for neutrons, slow and fast muons as well as contributions to the total production of 98.85%, 1.5% and 0.065%, respectively. These values are based on field-calibrated measurements (Braucher et al. 2003). A modern spallogenic production rate (i.e. induced by neutrons) of 4.49± 0.39 atoms g^{-1}year^{-1} at sea level and high latitude was used for internal consistency with the data of Stone (2000), according to the recently published absolute calibration of ^{10}Be AMS standards by Nishiizumi et al. (2007). Combined with contributions from slow and fast muons, this sea-level and high-latitude production rate has then been scaled for sampling altitudes and latitudes using the scaling factors proposed by Stone (2000).

The surface production rates were corrected for local slope and topographic shielding due to surrounding geomorphic features following Dunne et al. (1999). Analytical uncertainties (reported as 1σ; see Table 1 and Fig. 5) include a conservative 3% uncertainty based on long-term measurements of standards (Raisbeck et al. 1987, 1994), a 1σ statistical error on counted ^{10}Be events and the uncertainty associated with the chemical and analytical blank correction (associated ^{10}Be/^{9}Be blank ratio was $(3.86 \pm 1.72) \times 10^{-15}$). To compare the ^{10}Be exposure ages with absolute ages, an additional 6% maximum uncertainty for production rates was also systematically propagated (Stone 2000). Considering the geological context, the ^{10}Be ages were calculated assuming a negligible inherited component. We also considered the erosion negligible during the involved time period, and therefore provide minimum ages. Furthermore, as sample thicknesses were systematically <5 cm, no correction was applied for this effect. The presented data do not take into account temporal magnetic field variations as the induced effect on the production rates is assumed negligible on the time period spanned in this study (i.e. max. ~5% ^{10}Be production rate decrease compared to the modern value according to Pigati and Lifton 2004). CRE ages are thus presented in ^{10}Be-ka.

Results

Measured in situ-produced ^{10}Be concentrations ranging from 2.07 to 9.16×10^4 atoms g^{-1} yield CRE ^{10}Be ages ranging from 2.3±0.8 to 6.3± 1.6 ^{10}Be-ka (Table 1). As shown in Fig. 5, which presents the calculated CRE ages as a function of the sampling elevations, six of the seven measured samples yield ^{10}Be ages that statistically overlap. A first statistical treatment of these data was achieved using method described in Lowell (1995). Each CRE age obtained for each sample

Table 1 Sample locations, cosmogenic-nuclide analytical data and ^{10}Be exposure ages

Samples	Elevation (m)	Longitude WGS 84 (°E)	Latitude WGS 84 (°N)	Skyline shielding factor[a]	Corrected production rate (atoms g^{-1} year^{-1})[b]	^{10}Be concentration (10^4 atoms g^{-1})[c]	Exposure age (^{10}Be-ka)
Lau01	1,722	6.060	44.980	0.50	9.21±0.55	3.95±1.21	4.3±1.3
Lau04	1,513	6.069	44.974	0.93	14.65±0.88	9.16±2.34	6.3±1.7
Lau10	925	6.078	44.992	0.91	9.03±0.54	3.86±0.57	4.3±0.7
Lau11	887	6.078	44.993	0.94	8.93±0.54	2.07±0.70	2.3±0.8
Lau1800	1,800	6.075	44.977	0.75	14.59±0.88	5.71±1.42	3.9±1.0
Lau2025	2,025	6.075	44.977	0.63	14.46±0.87	8.83±1.51	6.1±1.1
Lau2075	2,075	6.072	44.978	0.63	14.97±0.90	7.56±1.99	5.1±1.4

[a] Geomorphic scaling factors calculated following the method of Dunne et al. (1999)

[b] Sample ^{10}Be production rate scaled for latitudinal and altitudinal effects from Stone (2000), using a modern spallogenic production at sea level and high altitude of 4.49±0.39 atoms g^{-1} year^{-1} (see text for details) and corrected from geomorphic factors

[c] Analytical uncertainties include a conservative 3% uncertainty based on long-term measurements of standards, a 1σ statistical error on counted ^{10}Be events and the uncertainty associated with the chemical and analytical blank correction (see text for details and references)

is considered as an individual Gaussian distribution with its value corresponding to the mean of the distribution and its associated uncertainty corresponding to the dispersion about the mean. Gaussian distributions of each individual CRE age can then be summed together to provide a new Gaussian distribution representative of the dataset (Lowell 1995). On Fig. 6a, the data probability curve shows a shoulder on the low-value side (i.e. from ~1.9 to ~2.9 ^{10}Be-ka), while a major mode appears at ~4.3 ^{10}Be-ka. To test the reliability of this major mode and in order to calculate an averaged age that takes into account individual age uncertainty, the mean square of weighted deviates (MSWD) statistic may be used (McIntyre et al. 1966; Douglass et al. 2006). By combining MSWD with probability curves, a group of samples sharing a common mean age may be identified (Douglass et al. 2006). A calculated MSWD value of 1.0 indicates that analytical errors are as expected, whereas a value less than 1.0 indicates that the analytical errors may be overestimated. Alternatively, a value significantly larger than 1.0 indicates either an underestimation of analytical errors or geological

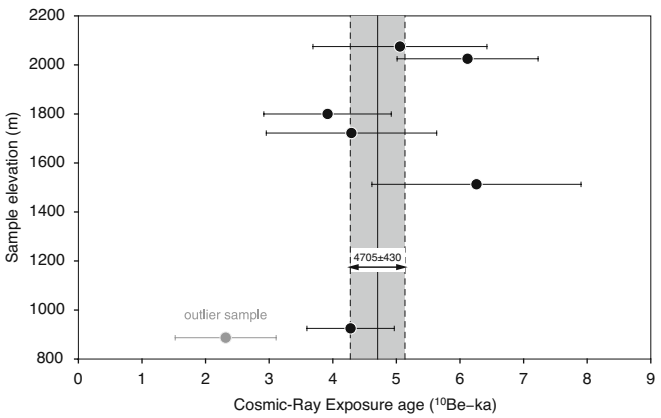

Fig. 5 Elevation distribution of Lauvitel rock avalanche samples. Samples' CRE ages are represented as well as 1σ uncertainties as a function of their sampling elevation. *Light grey shaded* sample corresponds to the outlier Lau11. Weighted CRE age (*solid vertical back line*) and its uncertainty (*grey shaded area*) calculated through the MSWD method is represented (see 'Sample preparation, analysis and cosmic ray exposure age calculation' and Fig. 6 for details)

factors producing dispersed CRE ages (Douglass et al. 2006). Considering all data, the MSWD value calculated is 1.78 and the weighted CRE age is 4.2±0.5 ^{10}Be-ka. When omitting sample Lau11, which causes the low-value shoulder observed on the cumulative probability curve (Fig. 6a), the MSWD value calculated for the six remaining samples is 0.74. Thus, Fig. 6b shows that by omitting sample Lau11, the new cumulative probability curve better fits a Gaussian distribution. Finally, it seems that the low-value shoulder shown on probability curve (Fig. 6a) identifies an outlier reflecting unusual geological processes, whereas the major mode highlights a single past collapse event at 4.7±0.4 ^{10}Be-ka.

Discussion

Three samples collected on blocks (i.e. Lau04, Lau10 and Lau11) are significantly younger than 10 ^{10}Be-ka and provide evidence that the material covering both the dam surface and the lower deposit is not glacial. The ages obtained for all samples except Lau11 are consistent with (but do not prove) the hypothesis of a single rock slide ~4.7 ^{10}Be-ka years ago. Lau11 corresponds to the most distant block and is located close to the Vénéon River, which erodes the toe of the deposit. This sample may have been buried in the deposit for some time before being exposed due to river bank erosion; this geological process may explain its younger age. Assuming this hypothesis, the estimated exposure age of the event is 4.7±0.4 ^{10}Be-ka (MSWD 0.74, n=6). For the reasons exposed below, no correction was applied for snow cover. The four samples Lau01, Lau1800, Lau2025 and Lau2075 have been collected in the scar where slopes are steeper than 55°. No correction was applied for these samples, as snow cover rarely accumulates on smooth rock slopes steeper than 45°. Although Lau04 was collected on an almost horizontal surface at about 1,500 m elevation within an area where snow cover is likely to reach 1 m during 4 months, this sample was taken on the top of a sharp >3-m-high block from which the snow is frequently blown, leading to limited snow thickness and persistence. Both Lau10 and Lau11 were sampled at an elevation of about 900 m where snow accumulation is moderate as well. Assuming a snow cover of 1 m during 4 months, which is an end-member scenario, would lead to a 220-years-older age. Therefore, we assume that this scenario would keep the consistence of a unique event ~4.7 ^{10}Be-ka ago, given reported uncertainties.

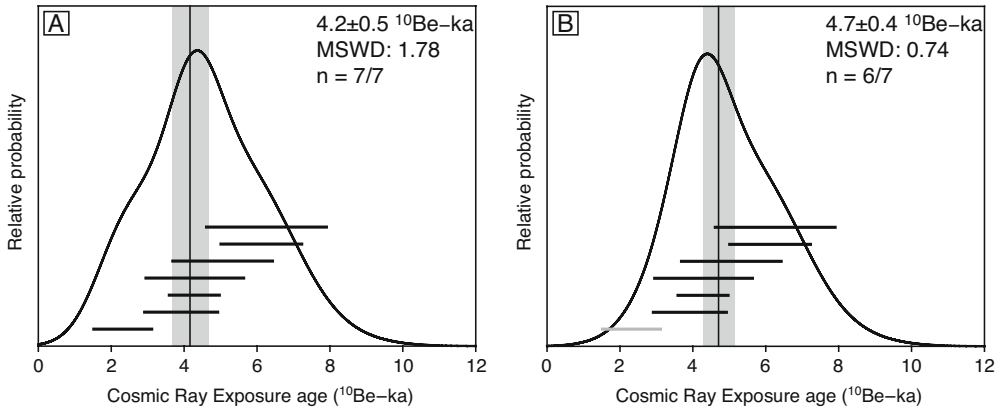

Fig. 6 CRE age probability spectra. (**A**) represents the cumulative probability curve computed from all data. (**B**) represents this cumulative probability curve considering only six of seven samples (Lau11 excluded, see 'Sample preparation, analysis and cosmic ray exposure age calculation' for details). *Thick horizontal bars* on each figure represent individual ages ($\pm 1\sigma$)

Our chronological results do not allow distinguishing more than one event, but the spatial distribution of the deposit shows two clearly separated areas (Fig. 2), which could hardly result from a unique movement. The reach angles of the two parts of the deposit can give some indications about the volume of the individual rock movements. Figure 7 (modified from Corominas 1996) shows the relation between the reach angle and volume for 47 slide events. This relation shows that a reach angle of 19°, which corresponds to the lower part of the Lauvitel deposit, can be attained only for a volume greater than about $10^7 m^3$. The only exception corresponds to unobstructed paths, which is not the case of the Lauvitel rock avalanche, as falling materials were deflected by the opposite valley wall. Therefore, the lower deposit may result from a large (or a few large) rock avalanche (s) with a volume larger than $10^7 m^3$. A reach angle of 33°, which corresponds to the upper part of the Lauvitel deposit, is highly improbable for a volume greater than $10^6 m^3$. Therefore, the upper deposit, whose volume has been estimated to at least $12 \times 10^6 m^3$ from geophysical prospecting, possibly results from the accumulation of individual rock movements smaller than $10^6 m^3$. However, neither CRE ages nor mechanical arguments allow constraining the chronology of individual rock movements (i.e. more dating should be necessary to define such a detailed chronology), but their occurrence in a narrow spatial and temporal scale shows a causal relation between successive events. From a probabilistic point of view, these rock movements cannot be considered independently and record a single multiphase event for rock fall/slide hazard assessment purposes. Furthermore, from a mechanical point of view, they could result from the previous large movement which produced the lower deposit, and probably occurred following a relatively short period of time. It must be recalled that a large volume of rock can fall in a short time period even by successive individual movements. Although the propagation distance is less than for a unique event, the risk can also be important. A recent example of successive rock movements making up a total volume of $\sim 30 \times 10^6 m^3$ in a few-hours timescale is given by the Randa rockslide (Sartori et al. 2003).

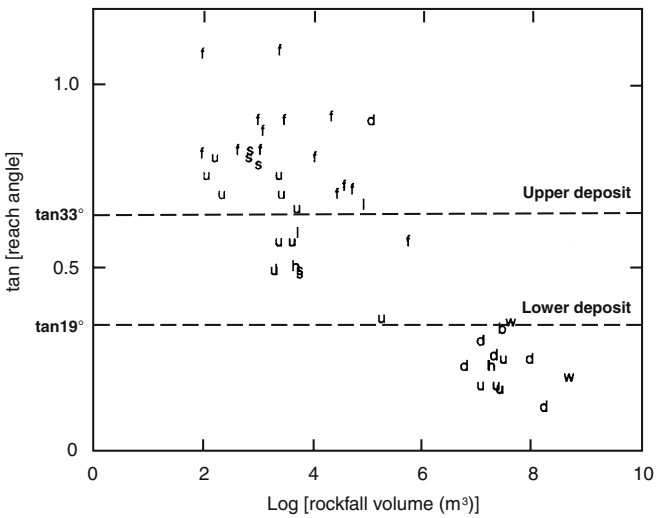

Fig. 7 Plot of rock fall and rock avalanche volume versus tangent of the reach angle for 47 events. Tangent of the reach angles of Lauvitel lower and upper deposits have been added. *Labels* correspond to obstacles and topographic constraints of the path: *f* dense forest, *s* scree deposit, *b* bends, *d* deflections, *h* channelling, *w* opposite wall, *u* unobstructed. Modified from Corominas (1996)

Conclusion

Electrical tomography allowed to confirm that the Lauvitel dam consists of a rock slide deposit and to estimate its volume at $12 \pm 4 \times 10^6 m^3$. The dam forms the upper part of a much larger rockslide deposit, whose total volume can be estimated to at least $50 - 70 \times 10^6 m^3$ from the apparent volume of the scar. The Abele (1974) hypothesis of a large rockslide–rock avalanche reaching the Vénéon River is consistent with (a) the systematic occurrence of large granite blocks on the surface of the deposit filling the bottom of the Vénéon valley, whereas the northern side valley walls of the Vénéon River are made of gneiss, (b) their ages that are much younger than expected in case of a glacial origin, (c) the existence of a sliding plane, the age of which overlaps that of the blocks downstream, (d) the size of the scarp and (e) the reach angle. This event might have occurred at $\sim 4.7 \pm 0.4$ ^{10}Be-ka but the hypothesis of several large events of more than $10^7 m^3$ cannot be rejected. More dating would be needed to confirm the uniqueness of this event. It can be inferred from the reach angle that the upper deposit, forming the Lauvitel dam, possibly results from successive individual rock movements smaller than $10^6 m^3$. In the context of rock fall hazard assessment for land use planning, all the movements described here have to be considered as a unique multiphase event dated at 4.7 ± 0.4 ^{10}Be-ka (MSWD 0.74, $n=6$) within a rock fall/slide inventory. Combining CRE dating and electrical tomography has proved to be an efficient tool to both date and characterise a Holocene rockslide–rock avalanche and contribute to further constrain the frequency of such catastrophic events.

Acknowledgements

This study is part of RD's Msc project at Université Paul Cézanne and Université Joseph Fourier in the framework of the ANCEMT project funded by the Agence Nationale de la Recherche (project N° 06-BLAN-0207). We thank the Parc National des Ecrins, X. Bodin, D. Fiat and O. Leroux for invaluable field assistance. We acknowledge S. Merkel and G. Aumaitre for technical assistance during ^{10}Be samples preparation and measurements, and P. van der Beek for improving the style of the manuscript. S. Garambois and A. Revil are also acknowledged for fruitful discussions on the interpretation of electrical prospecting results and D. Dumas for providing lake-level information. The geophysical survey was a low-carbon-footprint operation, with material transported by donkeys. A constructive review by an anonymous reviewer improved the manuscript.

References

Abele G (1974) Bergstürze in den Alpen. Ihre Verbreitung, Morphologie und Folgeerscheinungen. Wissenschaft Alpenvereinshefte 25, München

Ballantyne CK (2002) Paraglacial geomorphology. Quatern Sci Rev 21:1935–2017

Braucher R, Brown ET, Bourlès DL, Colin F (2003) In situ produced ^{10}Be measurements at great depths: implications for production rates by fast muons. Earth Planet Sci Lett 211:251–258

Brown ET, Edmond JM, Raisbeck GM, Yiou F, Kurz MD, Brook ED (1991) Examination of surface exposure ages of Antarctic moraines using in situ produced ^{10}Be and ^{26}Al. Geochim Cosmochim Acta 55:2269–2283

Claerbout JF, Muir F (1973) Robust modeling with erratic data. Geophysics 38:826–844

Climchalp (2008a) Climate change in the Alps: impacts and natural hazards. ONERC Technical Report N°1

Climchalp (2008b) State of knowledge on climate change impacts in the Alps. http://www.risknat.org/projets/climchalp_wp5/pages_eng/base_eng.htm

Corominas J (1996) The angle of reach as a mobility index for small and large landslides. Can Geotech J 33:260–271

Cossart E, Braucher R, Fort M, Bourlès DL, Carcaillet J (2008) The consequences of glacial debuttressing in deglaciated areas: pieces of evidence from field data and cosmogenic datings. Geomorphology 95:3–26

Cruden DM (1995) Rock slope movements in the Canadian Cordillera. Can Geotech J 22:528–540

Delebecque A (1898) Les lacs français. Chamerot & Renouard, Paris, p 436

Douglass DC, Singer BS, Kaplan MR, Mickelson DM, Caffee MW (2006) Cosmogenic nuclide surface exposure dating of boulders on last-glacial and late-glacial moraines, Lago Buenos Aires, Argentina: interpretive strategies and paleoclimate implications. Quatern Geochronol 1:43–58

Dunne J, Elmore D, Muzikar P (1999) Scaling factors for the rates of production of cosmogenic nuclides for geometric shielding and attenuation at depth on sloped surfaces. Geomorphology 27:3–11

Dussauge-Peisser C, Helmstetter A, Grasso JR, Hantz D, Desvarreux P, Jeannin M, Giraudet A (2002) Probabilistic approach to rock fall hazard assessment: potential of historical data analysis. Nat Hazards Earth Syst Sci 2:15–26

Fell R, Ho KKS, Lacasse S, Leroi E (2005) A framework for landslide risk assessment and management. In: Hungr O, Fell R, Couture R, Eberhardt E (eds) Landslide risk management. Taylor & Francis, London, ISBN 04 1538 043 X.: 3–25

Hantz D, Frayssines M (2007) Contribution à l'évaluation de la durée de vie d'un compartiment rocheux susceptible de s'ébouler. Rev Fr Géotech 119:65–79

Hantz D, Vengeon JM, Dussauge-Peisser C (2003) An historical, geomechanical and probabilistic approach to rock-fall hazard assessment. Nat Hazards Earth Syst Sci 3:693–701

Heim A (1932) Bergsturz und Menschenleben. Fretz & Wasmuth Verlag, Zurich, 218 pp.

Hormes A, Ivy-Ochs S, Kubik PW, Ferreli L, Maria Michetti A (2008) ^{10}Be exposure ages of rock avalanche and a late glacial moraine in Alta Valtellina, Italian Alps. Quatern Int 190:136–145

Hungr O, Evans SG (2004) The occurrence and classification of massive rock slope failure. Felsbau 22:1–11

Ivy-Ochs S, Poschinger AV, Synal H-A, Maisch M (2009) Surface exposure dating of the Flims landslide, Graubünden, Switzerland. Geomorphology 103:104–112

Kilian W (1922) Les stades de recul des glaciers alpins et l'origine du lac Lauvitel (Oisans). C R Acad Sci 175:660–665

Le Roux O, Schwartz S, Gamond JF et al (2009) CRE dating on the head scarp of a major landslide (Séchilienne, French Alps), age constraints on Holocene kinematics. Earth Planet Sci Lett 280:236–245

Lowell TV (1995) The application of radiocarbon ages estimates to the dating of glacial sequences: an example from the Miami sublobe, Ohio, USA. Quatern Sci Rev 14:85–99

McIntyre G, Brooks C, Compston W, Turek A (1966) The statistical assessment of Rb–Sr isochrones. J Geophys Res 71:5459–5468

Merchel S, Herpers U (1999) An update on radiochemical separation techniques for the determination of long-lived radionuclides via accelerator mass spectrometry. Radiochimica Acta 84:215–219

Monjuvent G (1978) Le Drac: morphologie, stratigraphie et chronologie quaternaire d'un bassin Alpin. Editions du CNRS, Paris, p 433

Moon AT, Wilson RA, Flentje PN (2005) Developing and using landslide frequency models. In: Hungr O, Fell R, Couture R, Eberhardt E (eds) Landslide risk management. Taylor and Francis, London, pp 681–690

Niklaus M (1967) Geomorphologische und limnologische Untersuchungen am Oeschinensee. Beiträge zur Geologie der Schweiz–Hydrologie, Nr 14. Bern

Nishiizumi K, Imamura M, Caffee MW, Southon JR, Finkel RC, McAninch J (2007) Absolute calibration of ^{10}Be AMS standards. Nucl Instrum Methods Phys Res, B Beam Interact Mater Atoms 258:403–413

Picarelli L, Oboni F, Evans SG, Mostyn G, Fell R (2005) Hazard characterization and quantification. In: Hungr O, Fell R, Couture R, Eberhardt E (eds) Landslide risk management. Taylor & Francis, London, ISBN 04 1538 043 X: 27–61

Pigati JS, Lifton NA (2004) Geomagnetic effects on time-integrated cosmogenic nuclide production with emphasis on in situ ^{14}C and ^{10}Be. Earth Planet Sci Lett 226:193–205

Prager C, Ivy-Ochs S, Ostermann M, Synal HA, Patzelt G (2009) Geology and radiometric ^{14}C-, ^{36}Cl-and Th-/U-dating of the Fernpass rockslide (Tyrol, Austria). Geomorphology 103:93–103

Raisbeck GM, Yiou F, Bourlès D, Lestringuez J, Deboffle D (1987) Measurements of ^{10}Be and ^{26}Al with a Tandetron AMS facility. Nucl Instrum Methods Phys Res, B Beam Interact Mater Atoms 29:22–26

Raisbeck GM, Yiou F, Bourlès D et al (1994) The AMS facility at Gif-sur-Yvette: progress, perturbations and projects. Nucl Instrum Methods Phys Res, B Beam Interact Mater Atoms 92:43–46

Sartori M, Baillifard F, Jaboyedoff M, Rouiller JD (2003) Kinematics of the 1991 Randa rockslides (Valais, Switzerland). Nat Hazards Earth Syst Sci 3:423–433

Schoeneich P, Hantz D, Deline P, Amelot F (2008) A new database of Alpine rock falls and rock avalanches. Interpraevent, Dornbirn, Austria 2:243–250

Soldati M, Corsini A, Pasuto A (2004) Landslides and climate change in the Italian Dolomites since the Late glacial. Catena 55:141–161

Stone JO (2000) Air pressure and cosmogenic isotope production. J Geophys Res 105:23753–23759

Van Husen D, Ivy-Ochs S, Alfimov V (2007) Landslides in Almtal: mechanism and age. Austrian J Earth Sci 100:114–126

R. Delunel (✉) · R. Braucher · D. L. Bourlès
Centre Européen de Recherche et d'Enseignement des Géosciences
de l'Environnement (CEREGE),
UMR 6635 CNRS–Aix Marseille Université, BP 80 13545 Aix en Provence, France
e-mail: romain.delunel@e.ujf-grenoble.fr

D. Hantz
Laboratoire de Géophysique Interne et de Tectonophysique,
Université Joseph Fourier, BP 53, 38041 Grenoble, France

P. Schoeneich
Institut de Géographie Alpine—UMR 5194-PACTE/Territoires,
Université de Grenoble, Grenoble, France

J. Deparis
BRGM,
3 avenue Claude-Guillemin, 45060 Orléans Cedex 2, France

Present address:
R. Delunel
Laboratoire de Géodynamique des Chaînes Alpines,
Université Joseph Fourier, BP 5338041 Grenoble, France